# Capillary pressure and buoyancy effects in the $CO_2$/brine flow system

J. S. Pau[1], W. K. S. Pao[1], S. P. Yong[2] & P. Q. Memon[2]
[1]*Department of Mechanical Engineering, Universiti Teknologi PETRONAS, Malaysia*
[2]*Department of Computer and Information Sciences, Universiti Teknologi PETRONAS, Malaysia*

## Abstract

The annual emission of $CO_2$ from human activities has exceeded the absorption abilities of nature. Carbon capture and geological storage is a solution that is able to combat the problem of excessive $CO_2$ release to the atmosphere, which endangers the lives of humans and all living things. Saline aquifer, which has a high permeability and storage capacity, has become a subject of interest as a $CO_2$ storage media. The flow of $CO_2$ into the aquifer initially occupied by saline water is the subject of study in this paper. Particularly, the effects of two significant parameters – capillary pressure and gravitational force have been considered. To solve the two phase flow equation, we have implemented the currently developed mixed and hybrid finite element method. The results show that capillary pressure enhance the flow of $CO_2$ whereas gravity force causes phase segregation with the less dense $CO_2$ flowing upward due to buoyancy forces.
*Keywords: capillary pressure, buoyancy effect, density segregation, $CO_2$/brine system.*

## 1 Introduction

Ever since the industrial revolution, power generation from fossil fuel has contributed in the increment of GHG [1]. Fossil fuel emission has contributed to 26% of total $CO_2$ emission [2]. The presence of a large amount of $CO_2$ has contributed to the greenhouse effect despite its low index in "Global Warming Potential" (GWP) [3]. There is approximately 24 Gt of $CO_2$ emitted from human activities annually – an amount that exceeds the natural absorption capacity of the ecosystem [4].

WIT Transactions on Ecology and The Environment, Vol 186, © 2014 WIT Press
www.witpress.com, ISSN 1743-3541 (on-line)
doi:10.2495/ESUS140541

The most promising way to combat the problem of excessive $CO_2$ release to the atmosphere is carbon capture and geological storage (CCGS) [1, 4] which comprise of capturing $CO_2$ from stationary sources, such as coal generation plants, transporting $CO_2$ to storage site and storing it for years [5]. Despite the immature understanding on practical risks posed by CCS, a few CCS projects are underway worldwide [6]. This technology is being pursued in North America, Northern Europe and Australia currently [7].

Impermeable layer such as the cap rock in the porous rock will trap the $CO_2$ and this is the most dominant trapping mechanism. Droplets $CO_2$ will resides in pore spaces for millions of years. To hold the $CO_2$ in porous rock securely for several hundreds of years, secondary trapping that involves dissolution and mineralization is critical important [8]. With these trapping mechanisms, $CO_2$ can be sequestrated in coal bed methane, deep saline aquifers, depleted oil and gas reservoir and ocean [3, 9]. Among these, deep saline aquifer provide the most ample storage capacity [10].

The pressure difference in between two immiscible fluids are known as capillary pressure. Capillary pressure curve has strong influence on the behaviour of the motion of fluid phase which enters an initially occupied porous medium by another fluid phase. Brooks and Corey [14] have presented their theory that relates saturation, pressure difference and the permeability of the two hydraulic fluids for porous media that saturates partially, based on Burdine's approach [18]. Theodoropoulou *et al.* [16] describe capillary function based on Corey's type of function and he provides both two equations for both drainage and imbibition condition.

A model of rectangular aquifer is set up as the analysis domain. The authors have used mixed and hybrid finite element method to discretize the two phase flow equation in order to study the effects of capillary pressure and gravitational effects on transport of $CO_2$ in saline aquifer. The results show that capillary pressure increase the flow rate of $CO_2$. The result corresponds to the finding by Goumiri *et al.* [15], 2011. The existence of gravity cause the segregation of $CO_2$ and brine due to the difference of density between them. The less dense $CO_2$ will tend to flow upward hence less saturation of $CO_2$ is found at the location near to the bottom of the aquifer. This result is found to be in parallel with Negara *et al.* 2011 [20] and Altundas *et al*. 2010 [10].

The aim of this research paper is to study the effects of capillary pressure and gravity force during $CO_2$ injection by solving the differential pressure and transport equations using mixed and hybrid finite element discretization method.

## 2 Mathematical modeling

### 2.1 Two phase flow

There are active interactions in between rock, and two fluid phases flow within the rock. The change of pressure within a differential in space is related to the interstitial velocity, $\boldsymbol{v}$ based on Darcy's law. By combining the continuity equation and Darcy's law, the pressure equation is obtained as [11].

$$\nabla \cdot \mathbf{v} = q, \quad \mathbf{v} = -\frac{\mathbf{K}}{\mu}\left(\nabla p + \rho g \nabla z\right) \tag{1}$$

Before the introduction of two-phase transport equation, the saturation concept has to be introduced. Saturation of each phases exist in the system is summed up to be unity.

$$S_w + S_g = 1 \tag{2}$$

As for a two-phase flow system that involves $CO_2$ as the gas phase and brine as water phase system, the transport equation is defined as [12]

$$\left.\begin{aligned} &\nabla \cdot \mathbf{v} = q, \quad \mathbf{v} = -\mathbf{K}\left(\lambda \nabla p + \left(\lambda_w \rho_w + \lambda_g \rho_g\right) g \nabla D\right) \\ &\phi \frac{\partial S_g}{\partial t} + \nabla \cdot \left(f_g \lambda_w \nabla p_c\right) + \nabla \cdot \left(f_g \mathbf{v}\right) = Q_g \end{aligned}\right\} \tag{3}$$

where $\rho_g$ and $\lambda_g$ are the density and mobility of $CO_2$ in gas phase and $f_g = \lambda_g / \lambda$ is fractional flow coefficient. Note that the subscript, $g$ is used for gas phase $CO_2$ whereas the subscript $w$ is used for water phase, brine.

### 2.2 Capillarity and capillary pressure

Capillarity is the result of combined effects of cohesive and adhesive forces. Cohesive force is an intermolecular forces between the same type particles. It causes surface tension and hence, a curved surface. Adhesive is an intermolecular force between different types of particles. According to [13], capillary pressure curve has a strong influence on the behaviour of the solution. Capillary pressure is the pressure difference between two fluids that form an interface [14, 15]. Proportional to the surface tension, the capillary pressure for water gas system is defined as [14],

$$P_c = P_g - P_w = \left(\rho_g - \rho_w\right) g h \tag{4}$$

where $\rho_g$ and $\rho_w$ represents the density of gas and water respectively, $g$ is the gravitational acceleration and $h$ is the height of the fluid column.

Brooks and Corey [14] have established an analytical model for capillary pressure, which becomes one of the most often used model. To describe in mathematical form

$$S_{ew} = \begin{cases} \left(p_c / p_e\right)^{-n_b} & p_c > p_e \\ 1 & p_c \le p_e \end{cases} \tag{5}$$

$$p_c = p_e \left(S_{ew}\right)^{-1/n_b} \tag{6}$$

where $p_e$ is denotes the entry pressure of air and $n_b$ is a parameter for pore-size distribution. $S_{ew}$ represents the normalized water phase saturation, as in mathematical form

$$S_{ew} = \frac{S - S_{rw}}{1 - S_{rw}}$$

Theodoropoulou has developed the function for capillary pressure by following Corey type functions. For primary drainage processes where non-wetting phase displacing the wetting-phase [16],

$$P_c = P_c^0 \left( 1 - \frac{S_{nw}}{1 - S_{wi}} + b_c \right)^{-m_c} \tag{7}$$

The irreducible wetting phase saturation is $S_{wi} (0 \le S_{nw} \le 1 - S_{wi})$.

As for primary imbibition process where wetting-phase displaces the non-wetting phase,

$$P_c = P_c^0 \left( 1 - \frac{S_{nw}}{1 - S_{nwr}} + b_c \right)^{-m_c} \tag{8}$$

The residual non-wetting phase saturation is $S_{nwr} (0 \le S_w \le 1 - S_{nwr})$.

Fig. 1 illustrates the capillary pressure curve with respect to $CO_2$ saturation. There is a peak curve at a high saturation point for both models, which is at $S_w \approx 0.95$ with the residual of water saturation set as $0.05$. This is due to the nature of the equation and depending on the constant parameters. For instance, the value of pore-size distribution parameter and residual saturation of water will affect the point of peak capillary pressure. In current work, we monitor the effect of capillary pressure based on Theodoropoulou's drainage model on $CO_2$ distribution. The alternating drainage and imbibition condition which leads to hysteresis effect of capillary pressure has been neglected.

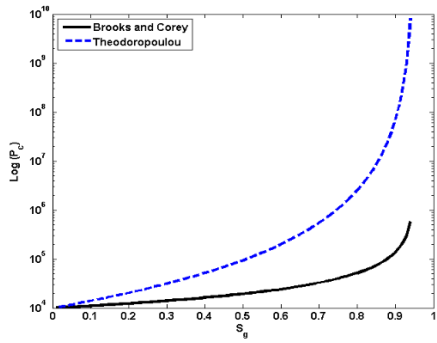


Figure 1: Capillary pressure plot based on Brooks and Corey's model and Theodoropoulou's.

### 2.3 Porosity, permeability and relative permeability

Porosity is one of the most important rock properties and it describe the fraction of total rock volume to pore space. In mathematical terms,

$$\phi = \frac{V_p}{V_t} \tag{9}$$

Total porosity in a rock includes the interconnected and isolated pores whereas effective porosity includes only the former [17]. Connected pores allow fluid to flow through. More connected pores in rock has higher capacity to permit fluid flow and this is measured by the parameter absolute permeability. Permeability depends on porosity and grain-size distribution. However, a porous rock does not necessarily high in permeability.

Brooks and Corey model is based on the combination of Corey's and Burdine's equation [18]. Brooks and Corey's model is expressed mathematically as [14]

$$k_{rw}\left(S_g\right) = \left(1 - S_{eg}\right)^{\frac{2+3\lambda}{\lambda}} \tag{10}$$

$$k_{rg}\left(S_g\right) = S_{eg}^2\left[1 - \left(1 - S_{eg}\right)^{\frac{2+\lambda}{\lambda}}\right] \tag{11}$$

$\lambda$ denotes the index for pore size distribution whose value changes based on the type of material. For instance, $\lambda = 0.2$ for heterogeneous material whereas $\lambda = 2.0$ for homogeneous material [19]. $S_{eg}$ is the normalized gas phase saturation, defined as [20]

$$S_{eg} = \frac{S - S_{rg}}{1 - S_{rg} - S_{rw}}$$

The residual saturation are represented as $S_{rg}$ (for gas phase) and $S_{rw}$ (for water phase).

### 2.4 Treatment of boundary conditions

The primary unknown from the two phase flow equation is *S* (saturation). The rectangular domain is bounded by four boundaries. Neumann boundary is set for all the four boundaries of the rectangles. In mathematical terms,

$$p_w = p_D, x \in \Gamma_D$$
$$\mathbf{v} \cdot \hat{n} = q_N, x \in \Gamma_N$$

$p_D$ is the pressure on $\Gamma_D$, $q_N$ is the flow rate on $\Gamma_N$ and $\hat{n}$ is the normal vector on the boundary.

## 3 Discretization of 2 phase flow equations

The currently developed mixed and hybrid finite element method is implemented. According to [12], the cell based discretization for Darcy's law can be expressed as

$$\mathbf{Mu} = \mathbf{e}p_i - \boldsymbol{\pi},\ \mathbf{e} = \left(1,\ldots,T\right)^T,\ \ \mathbf{u} = \mathbf{T}\left(\mathbf{e}p_i - \boldsymbol{\pi}\right) \tag{12}$$

The local inner product **M** and transmissibility matrix **T** are inverse of one another. $\boldsymbol{u}$ is the flux outward of cell faces, $\boldsymbol{\pi}$ denotes the pressure at the discrete cell faces whereas $p$ denotes the pressure at the discrete cell center. The flux and pressure drop can be written in tensor notation form as

$$u_k = -n_k \mathbf{Ka},\ \ p_i - \pi_j = c_{ik} \cdot \mathbf{a} \tag{13}$$

By using hybridized mixed form discretization, the flux continuity and pressure across the cell and face in linear system is described in block-matrix equation as [12, 21]

$$\begin{bmatrix} \mathbf{B} & \mathbf{C} & \mathbf{D} \\ \mathbf{C}^{\mathbf{T}} & 0 & 0 \\ \mathbf{D}^{\mathbf{T}} & 0 & 0 \end{bmatrix} \begin{Bmatrix} \mathbf{u} \\ -p \\ \boldsymbol{\pi} \end{Bmatrix} = \begin{Bmatrix} 0 \\ q \\ 0 \end{Bmatrix} \tag{14}$$

The discretization of Darcy's law is represented in the first row of the block-matrix. As for the second row, it describes the mass conservation and the third raw is the continuity of fluxes at cell faces. The matrix in eqn. (13) can be solved using Schur-complement system. The face pressure is obtained as

$$\left(\mathbf{D}^T\mathbf{B}^{-1}\mathbf{D} - \mathbf{F}^T\mathbf{L}^{-1}\mathbf{F}\right)\boldsymbol{\pi} = \mathbf{F}^T\mathbf{L}^{-1}\mathbf{q} \tag{15}$$

where $\mathbf{F} = \mathbf{C}^T\mathbf{B}^{-1}\mathbf{D}$ and $\mathbf{L} = \mathbf{C}^T\mathbf{B}^{-1}\mathbf{C}$. Using back substitution, cell pressures and fluxes are solved using

$$\mathbf{Lp} = \mathbf{q} + \mathbf{F}\boldsymbol{\pi},\ \ \mathbf{Bu} = \mathbf{Cp} - \mathbf{D}\boldsymbol{\pi} \tag{16}$$

The discretization of two phase flow is based on upstream-mobility weighing scheme. Eqn. (2) is discretized as

$$\begin{aligned} S_i^{n+1} = S_i^n + \frac{\Delta t}{\phi_i |c_i|}\left(\max\left(q_i, 0\right) + f\left(s_i^m\right)\min\left(q_i, 0\right)\right) - \\ \frac{\Delta t}{\phi_i |c_i|}\left(\sum_j \left[f\left(s_j^m\right)\max\left(v_{ij}, 0\right) + f\left(s_j^m\right)\min\left(v_{ij}, 0\right)\right]\right) \end{aligned} \tag{17}$$

## 4 Model Setup

A rectangular model of $50m \times 40m \times 1m$ is created as shown in Fig. 2. This aquifer model is generated similarly to that used by [20]. The model consists of 2000 grid blocks. Initially, brine water filled up the aquifer. The boundary condition of the aquifer is shown in fig. 2. A constant injection of $1PVI$ / *year* is set for one year. The porosity and permeability of the aquifer are presumed to be 0.2 and 1.0mD. For the rest of the fluid properties are shown in Table 1. We assume that the residual $CO_2$ and brine water saturation is at 0. The injection well is located at the bottom left corner of the rectangular domain and the production well is located at the top right corner of the domain, as shown in fig. 2.

Table 1: Aquifer properties.

| Parameters | Values |
|---|---|
| Viscosity of gas, $\mu_g \left(kgm^{-1}s^{-1}\right)$ | 0.0592 |
| Viscosity of water, $\mu_w \left(kgm^{-1}s^{-1}\right)$ | 0.6922 |
| Density of gas, $\rho_g \left(kgm^{-3}\right)$ | 716.7000 |
| Density of water, $\rho_w \left(kgm^{-3}\right)$ | 997.4200 |
| $S_{rg}$ | 0.001 |
| $S_{rw}$ | 0.05 |

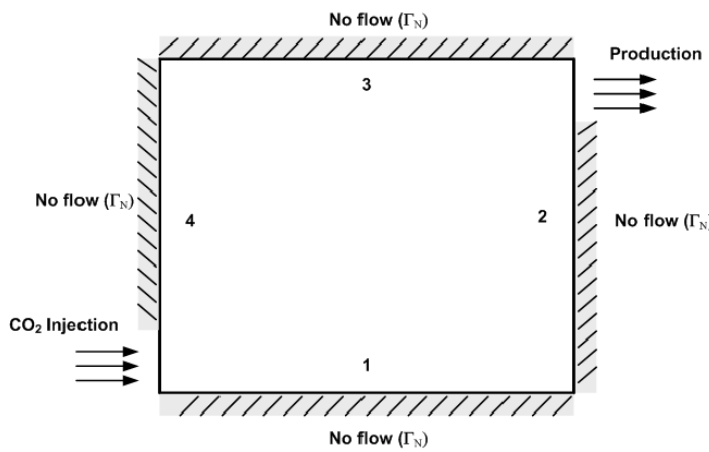


Figure 2: Boundary condition treatments of the domain.

## 5 Results and discussion

The result of $CO_2$ plume in two dimensional homogeneous porous media is presented. We simulate four cases including neglecting the gravity and capillarity, with only the gravity, with only the capillary pressure and with both gravity and capillary pressure for two-phase incompressible flow. The domain is sized to $50\text{m} \times 40\text{m} \times 1\text{m}$, in x and z axes, discretized into 2000 uniform mesh.

Figs 3 and 4 shows the $CO_2$ saturation distribution for the four cases. It is clear that the saturation is high near the injection point and dispersed radially outward toward the production point. For a closer view on the exact decrement of $CO_2$ saturation from injection point, we plotted the saturation in one dimensional at the depth of 1m, as in fig. 5. There is a pronounced drop of $CO_2$ saturation at the distance of 25m to 30m for all four cases. The result is found to have similar saturation change trend with [20, 22, 23]. Fig. 3(a) shows the case without considering gravity and capillary pressure. The highest $CO_2$ saturation is found to be 0.865 for this case. With the existence of gravity, $CO_2$ saturation near the bottom of the aquifer domain is slightly decreased, as seen in fig. 3(b) in 2D plot and in in fig. 5 in 1D plot. This could be due to the density segregation induced by the gravity where $CO_2$ tend to flow above the brine due to its lower density. This is said to be the buoyancy effect caused by the difference in density during two phase flow [20]. The highest saturation which occurs at the cell nearest to injection point is 0.864.

Fig. 4 shows the 2D plot for the case with capillary pressure. For a closer view in in fig. 5, the highest saturation which occurs at the cell nearest to injection point is found to be 0.949 (for the case without gravity) and 0.948 (for the case with gravity). Similar to the result of in fig. 3, gravity has cause a buoyancy force and the saturation at near bottom of the aquifer is decreased. With the existence of capillary pressure, the saturation of $CO_2$ near to the injection well is higher compare to the case without capillary pressure. The slope of the saturation curve for the case with capillary pressure is straighter but steeper compare to the case without capillary pressure. Capillary pressure is able to "push" the $CO_2$ to a distance further, for instance, 32m at the depth of 40m. This result corresponds to the finding by [15, 25]. They concluded that the extension of the plume at the beginning of the injection could be explained by the concept of capillary pressure. Capillary causes the saturation to spreads out at the front of the plume but its overall effect on overall plume size is negligible.

At the depth of 36m, the trend of $CO_2$ saturation distribution is similar to the one at the depth of 40m. However, the effect of gravity is less as compare to the condition at depth of 40m, for both case with and without capillary pressure. The highest $CO_2$ saturation for each case is 0.6304 (no g and no Pc), 0.6285 (with g but no Pc), 0.7883 (no g but with Pc) and 0.7827 (with g and Pc).

At the depth near to the top of aquifer domain, i.e. 15m, there are remarkable change in the $CO_2$ distribution when compared to the case deeper in the aquifer. The presence of gravity force increase the $CO_2$ distribution rate at this depth, as in in fig. 7. In addition to this, the presence of capillary pressure has increased the flow rate of $CO_2$.

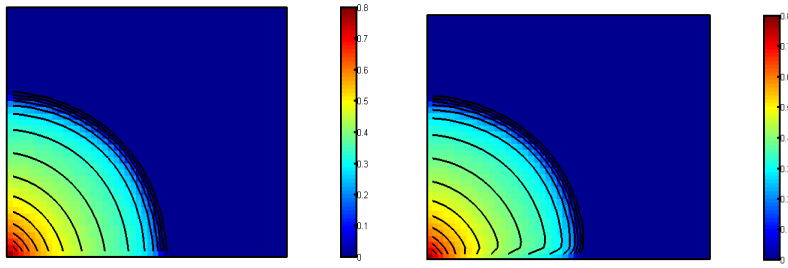

(a) (b)

Figure 3: 2D simulation of (a) the case without gravity and capillary pressure; (b) the case with gravity and without capillary pressure.

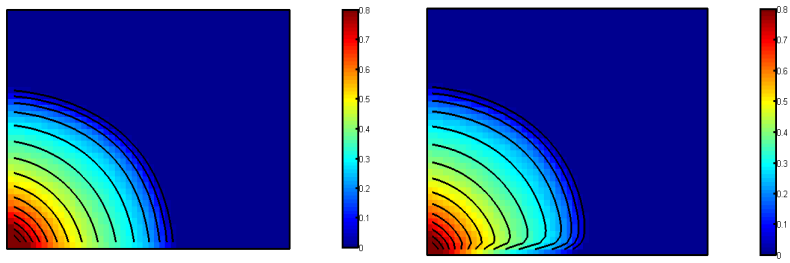

(a) (b)

Figure 4: 2D simulation of the case (a) without gravity but with capillary pressure; (b) with both gravity and capillary pressure.

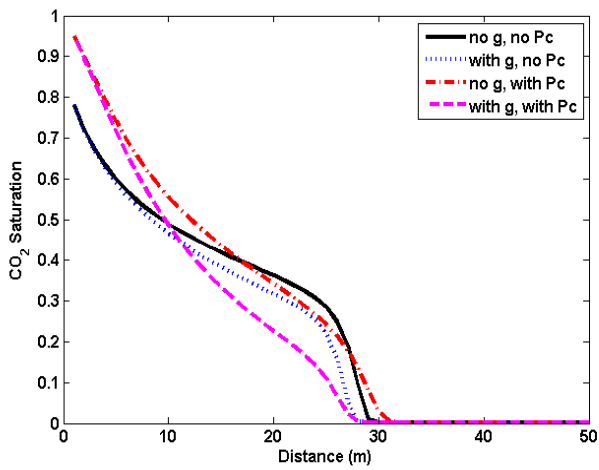


Figure 5: 1D plot of cell at depth 40m.

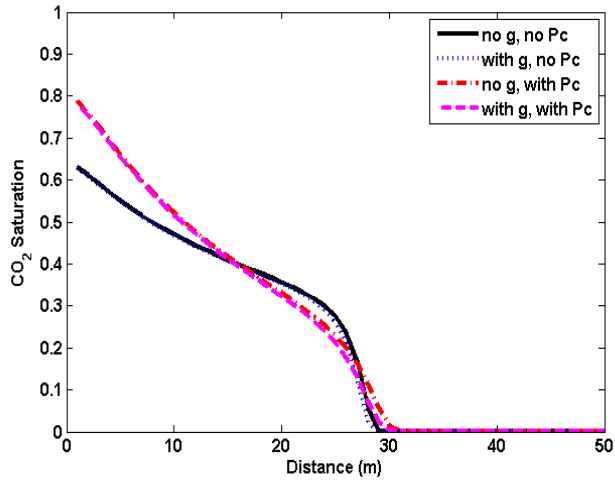


Figure 6: 1D plot of cell at depth 36m.

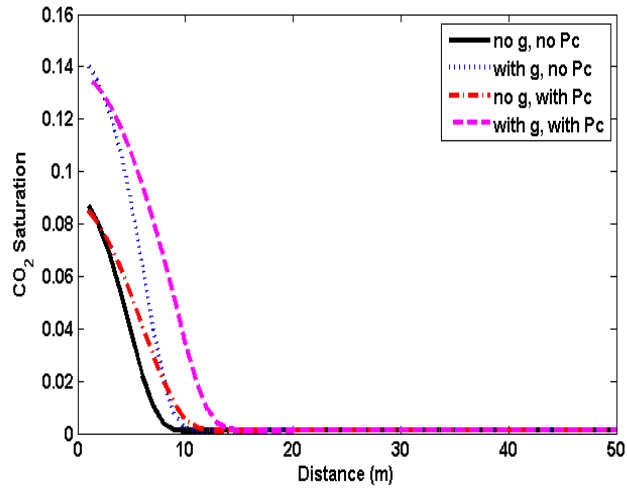


Figure 7: 1D plot of cell at depth 15m.

## 6 Conclusions

This paper is the presenting the study on $CO_2$ injection in homogeneous saline aquifer. Two phases – $CO_2$ and brine are considered to exist only in the aquifer. The injection of $CO_2$ into the aquifer with brine will replace brine to fill up the porous media. Numerical implemented to solve the two phase flow equation is

mixed and hybrid finite element method. The flow of $CO_2$ is radially outward away from the injection point, towards the production outlet. The effect of gravity and capillary pressure are different depending on the depth of the saline aquifer. The effect of gravity that leads to buoyancy has cause a decrement of $CO_2$ saturation, especially at the depth of 40m. At this depth, capillary pressure act as an additional force that push $CO_2$ forward. However, at the depth near to the top, i.e. 15m, the presence of gravity increase the flow of $CO_2$ and so as capillary pressure.

## Acknowledgement

The authors would like to thank UTP EOR MOR for their financial support on this research via YUTP 015-3AA-A65.

## References

[1] International Energy Agency (IEA/OECD), "Prospects for $CO_2$ Capture and Storage," Paris, France, 2004.

[2] IPCC, *Climate Change: The Physical Science Basis. Contribution of Working Group 1 to the Fourth Assessment Report of the Intergovernmental Panel on Climate Change,* Cambridge University Press, Cambridge, UK, 2007.

[3] Scharf, S. & Clemens, T., CO2-Sequestration Potential in Austrian Oil and Gas Fields," in SPE Europe/EAGE Annual Conference and Exhibition, Society of Petroleum Engineers, Vienna, Austria, 2006.

[4] Freund, P., International Developments in Geological Storage of $CO_2$, in Exploration Geophysics, **37**, pp. 1-9, 2006.

[5] Mathias, S., Miguel, G.J., Thatcher, K.E. & Zimmerman, R.W., Pressure Buildup During CO2 Injection into a Closed Brine Aquifer. *Transp Porous Media*, **89**, pp. 383-397, 2011.

[6] Damen, K., Faaij, A. & Turkenburg, W., Health, Safety and Environment Risks of Underground CO2 Storage – Overview of Mechanisms and Current Knowledge. *Climate Change*, **74**, pp. 289-318, 2006.

[7] Bachu, S. & Bennion, B., Effects of In-Situ Conditions on Relative Permeability Characteristics of $CO_2$-Brine System. *Environmental Geology*, **54(8)b**, pp. 1707-1722, 2008.

[8] Nordbotten, J., Celia M. & Bachu, S., Injection and Storage of CO2 in Deep Saline Aquifers: Analytic Solution for $CO_2$ Plume Evolution during Injection. *Transport Porous Media*, 70, pp. 339-360, 2005.

[9] Bachu, S., Bonijoly, D., Bradshaw, J., Burruss, R., Holloway, S., Christensen, N.P. & Mathiassen, O.M., CO2 Storage Capacity Estimation: Methodology and Gaps. *International Journal of Greenhouse Gas Control*, **1**, pp. 430-443, 2007.

[10] Altundas, Y.B., Ramakrishnan, T.S., Chugunov, N. & deLoubens, R., Retardation of $CO_2$ due to Capillary Pressure Hysteresis: A New $CO_2$ Trapping Mechanism. SPE International Conference on $CO_2$ Capture, Storage and Utilization, 2010.

[11] Brezzi, F. & Fortin, M., Mixed and Hybrid Finite Element Methods. *Computational Mathematics*, Springer, New York, 1991.
[12] Lie, K.A., Krogstad, S., Ligaarden, I.S., Natvig, J.R., Nilsen H.M. & Skaflestad, B. Open-source MATLAB Implementation of Consistent Discretisations on Complex Grids. *Computer Geoscience*, pp. 297-322, 2012.
[13] Brenner, K., Cancès, C. & Hillhorst, D, Finite Volume Approximation for an Immiscible Two-Phase Flow in Porous Media with Discontinuous Capillary Pressure. *Computer Geosicence*, pp. 573-597, 2013.
[14] Brooks, R.H. & Corey, A.T., Hydraulic Properties of Porous Media. *Hydrogeology Papers*, Colorado State University Fort Collins, Colorado, pp. 27, 1964.
[15] Goumiri, I.R., Prévost J.H. & Preisig, M., The Effect of Capillary Pressure on the Saturation Equation of Two-Phase Flow in Porous Media. *International Journal for Numerical and Analytical Methods in Geomechanics*, 2011.
[16] Theodoropoulou, M.A., Sygouni, V., Karoutsos V. & Tsakiroglou, C.D., Relative Permability and Capillary Pressure Functions of Porous Media as Related to the Displacement Growth Pattern. *International Journal of Multiphase Flow*, **31(10-11)**, pp. 1155-1180, 2005.
[17] Chen, Z., Reservoir Simulation – Mathematical Techniques in Oil Recovery. Society for Industrial and Applied Mathematics, 2007.
[18] Burdine, N.T., Relative Permeability Calculations from Pore-Size Distribution Data. *Trans AIME*, 1952.
[19] Mualem, Y., A New Model for Predicting the Hydraulic Conductivity of Unsaturated Porous Media. *Water Resource Research*, **12(3)**, 1976.
[20] Negara, A., Fathy E-Amin M. & Sun S., Simulation of $CO_2$ Plume in Porous Media: Consideration of Capillarity and Buoyancy Effects. *International Journal of Numerical Analysis and Modeling*, Series B, **2(4)**, pp. 315-337, 2011.
[21] Aarnes, J.E., Krogstad, S. & Lie, K.A., Multiscale Mixed/Mimetic Methods on Corner-Point Grids. *Computational Geoscience*, **12(3)**, pp. 297-315, 2008.
[22] Piri, M., Prevost, J.H. & Fuller, R., Carbon Dioxide Sequestration in Saline Aquifers: Evaporation, Precipitation and Compressibility Effects. Fourth Annual Conference on Carbon Capture and Sequestration DOE/NETL, 2005.
[23] N. Muller, R. Qi, E. Mackie, K. Pruess and M.J. Blunt, "CO2 Injection Impairment due to Halite Precipitation," in Energy Procedia 1, 2009, pp. 3507-3514.